Influence of voids on the engineering constants of paper

Part 2: Void modeling

Lakshmikanthan Subramanian and Leif A. Carlsson

ABSTRACT: This is the second part of a two-part study into the influence of voids on the elastic properties of paper. Voids in the paper sheet are modeled as regularly distributed inclusions (with zero elastic properties) embedded in an isotropic or orthotropic matrix. The elastic stiffnesses of isotropic materials containing different shapes and volume fractions of voids were analyzed using Christensen's three-phase self-consistent models. Voids in an orthotropic matrix were analyzed using two- and three-dimensional finite-element analysis, and the results were correlated with available experimental data.

KEYWORDS: Chemical pulps, coefficients, elasticity, engineering, finite element analysis, hygroexpansivity, mechanical properties, models, paper, voids.

The formation of paper from a suspension of fibers results in a relatively loosely packed sheet. The apparent density of the sheet increases during the pressing and calendering operations, but the final sheet still contains a substantial volume occupied by voids. The presence of voids in the sheet reduces its elastic moduli. Thus any micromechanical modeling of paper would be incomplete unless attention is given to the void or pore structure *(1)*.

Micromechanical theories of paper can be grouped as either network models or continuum models, as noted in Part 1 of this paper *(2)*. While continuum models *(3)* completely ignore the presence of voids, elastic moduli calculated from network models are commonly scaled with a factor ρ_S/ρ_C, where ρ_S is the apparent density of the sheet and ρ_C is the density of the cell-wall material *(4)*. As will be discussed in this study, such a correction tends to be unconservative and is not supported by more refined analyses of voids.

Corte *(5)* proposed that the gaps between the fibers in the paper form a minute pore system that can be viewed as tiny cylinders extending through the thickness of the sheet. The size distribution of pores can be measured by a mercury-intrusion method. **Figure 1** presents pore size distributions measured by Corte *(5)* for papers made from unbleached kraft pulp beaten to various degrees. It is evident that the mean pore diameter is on the order of 1–2 μm, which is much smaller than the planar dimensions of the fibers. Figure 1 also shows that increased beating reduces the mean pore size and sharpens the distribution.

Analyses of the influence of the pores on the effective mechanical properties of paper are extremely rare. Salmen and Rigdahl *(6)* assumed that the voids in a sheet of paper can be modeled as spherical inclusions within an isotropic matrix. They used semiempirical equations to calculate the effective elastic constants of porous materials.

In the present study, self-consistent micromechanical models and finite-element analysis are used to determine the influence of voids on the engineering constants of isotropic and orthotropic paper sheets. The baseline orthotropic elastic constants of papers with no voids are calculated from the laminate model that was presented in Part 1 *(2)*. The analysis of voids presented here in

Subramanian, graduate student, and Carlsson, professor, are affiliated with the Dept. of Mechanical Engineering, Florida Atlantic University, Boca Raton, FL 33431.

1. Distribution of pore sizes at three levels of refining in papers produced from unbleached kraft pulp *(5)*

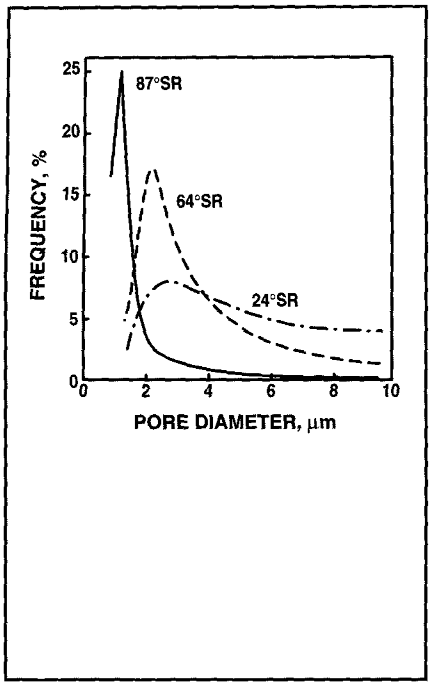

2. Microstructure of paper produced from bleached chemical pulp

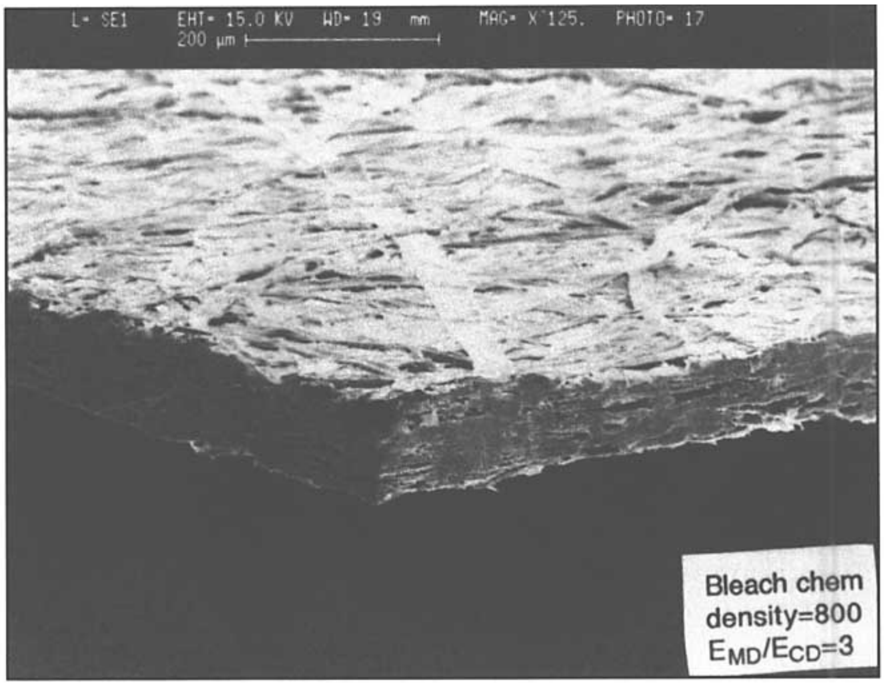

Part 2 quantifies the appropriate reduction factors for the elastic constants. After appropriate scaling, the model predictions are compared with some available experimental data in the literature.

Void modeling

Modeling the mechanical response of paper is complicated by the complexity of the sheet structure. **Figure 2** is a magnified photograph of a paper sheet. Examination of Fig. 2 reveals wide spectrums of size, shape, and relative orientation of the fibers and void structure *(5)*. To develop tractable micromechanical solutions relating structural features and fiber properties to the macroscopic behavior of paper, idealized models have to be constructed and analyzed. We will present some available micromechanical approaches and apply finite-element analysis to assess the influence of voids on the elastic and hygroexpansional properties of paper.

Composite-spheres model

Hashin and Rosen *(7)* developed the "composite spheres" model to obtain the elastic properties of macroscopically isotropic two-phase materials. The model is composed of a gradation of sizes of spherical particles (inclusions) embedded in a continuous matrix phase such that a volume-filling configuration is achieved. This model would be expected to give reasonable results for systems containing spherical inclusions with a wide distribution of sizes. For paper, however, the pores are approximately cylindrical, as described by Corte *(5)*, which renders this model less useful for modeling of paper.

Three-phase self-consistent model

Christensen and Lo *(8)* derived exact solutions for the engineering constants of isotropic media containing spherical or cylindrical inclusions. The material is assumed to consist of three phases: the inclusions (spheres or infinitely long aligned cylinders of varying diameters such that volume filling is achieved), a spherical or cylindrical shell of matrix surrounding the inclusions, and the continuous equivalent homogeneous media in which the inclusions are embedded. The geometry of a material with cylindrical inclusions is shown in **Fig. 3**. Notice that this model represents isotropic sheets with through-thickness pores *(5)*.

Although of less interest for this study, Christensen and Lo's model *(8)* also provides the properties in the thickness direction (*z*-direction). It can be easily shown that Young's modulus and Poisson's ratio in the *z*-direction (E_z and ν_z) follow the simple linear rule of mixtures, i.e.,

$$E_z/E_m = \nu_z/\nu_m = 1 - V_P \qquad (1)$$

where subscript "m" represents the continuous-matrix phase and V_P is the volume fraction of pores (voids) in the sheet. **Table I** summarizes the results for isotropic materials with spherical and cylindrical void inclusions.

To obtain the in-plane shear modulus, G, from the data listed in Table I, the following equation can be used.

$$G = E/[2(1+\nu)] \qquad (2)$$

3. Cylindrical through-thickness inclusions

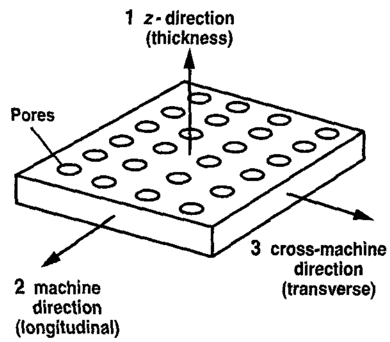

I. Engineering constants of an isotropic material containing spherical and cylindrical voids

	Spherical voids		Cylindrical voids	
V_P	E/E_m	ν/ν_m	E/E_m	ν/ν_m
0.0	1.000	1.000	1.000	1.000
0.1	0.814	0.957	0.773	1.049
0.2	0.658	0.929	0.587	1.126
0.3	0.519	0.914	0.428	1.268
0.4	0.398	0.911	0.285	1.511
0.5	0.295	0.920	0.164	1.883
0.6	0.209	0.935	0.073	2.353
0.7	0.139	0.957	0.022	2.757
0.8	0.083	0.978	0.004	2.975

* Calculated from Christensen and Lo's three-phase models *(8)*

Comparison of the results for spherical and cylindrical voids in Table I reveals that cylindrical voids result in larger modulus reductions than spherical voids. Furthermore, Poisson's ratio for a material with spherical voids is approximately equal to that of the host matrix, but it exceeds that of the matrix for a material with cylindrical voids.

Finite-element modeling of voids

Part 1 *(2)* presented a laminate model that generates the in-plane elastic constants for void-free orthotropic paper sheets. The orthotropy of the constituent matrix considerably increases the complexity of the micromechanical analysis of the influence of voids, and no such analysis is readily available. The analysis of voids in an orthotropic matrix therefore is based on a numerical solution of certain boundary-value problems defined in terms of specific phase geometries.

The finite-element method has been found suitable for determining the effective mechanical properties of composite materials with regular packing and uniform size and shape of the inclusions *(9–11)*. While it is clear that the voids in paper sheets are not regularly packed and possess wide spectra of sizes and shapes (see Fig. 2), a tractable numerical solution requires the assumptions of uniform size and shape and regular packing of the voids. Modeling of the local inelastic response of fiber-reinforced composites is sensitive to the details of the repeat arrangement, as noted by Christman *et al.* *(11)*, but global (averaged) elastic properties are less sensitive to the packing geometry.

Figure 4 shows the representative volume elements (RVEs) for materials with cylindrical and spherical voids. The theoretical maximum volume fractions for materials containing regularly spaced cylindrical and spherical voids of uniform size are 0.78 and 0.52, respectively.

Two-dimensional finite-element analysis

The RVE of a material with through-the-thickness pores (Figs. 3 and 4A) can be discretized using two dimensional (2-D) finite elements, as seen in **Fig. 5**. Given the symmetries in geometry and loading, only one fourth of the RVE needs to be considered. Note that the x and y directions correspond to the machine direction (MD) and the cross-machine direction (CD), respectively.

Four-noded STIF 42 quadrilateral plane stress elements (stress $\sigma_z = 0$) with two translational degrees of freedom at each node were employed in the finite-element analysis *(12)*. A fine mesh was constructed near the void boundary to capture the steep stress and strain gradients. The side length of the smallest elements was $a/20$, where a is half the RVE side length. Volume fractions of pores ranging from 0.1 through 0.7 (in steps of 0.1) were considered using 189 nodes and 160 elements for all volume fractions of pores. The elastic constants for the isotropic and orthotropic paper sheets were generated by the laminate model described in Part 1 *(2)*.

Tensile loading and boundary conditions applied on the RVE are shown in **Fig. 6A**. A generalized plane strain

4. RVEs for materials with two types of voids. **A:** cylindrical pores, **B:** spherical voids

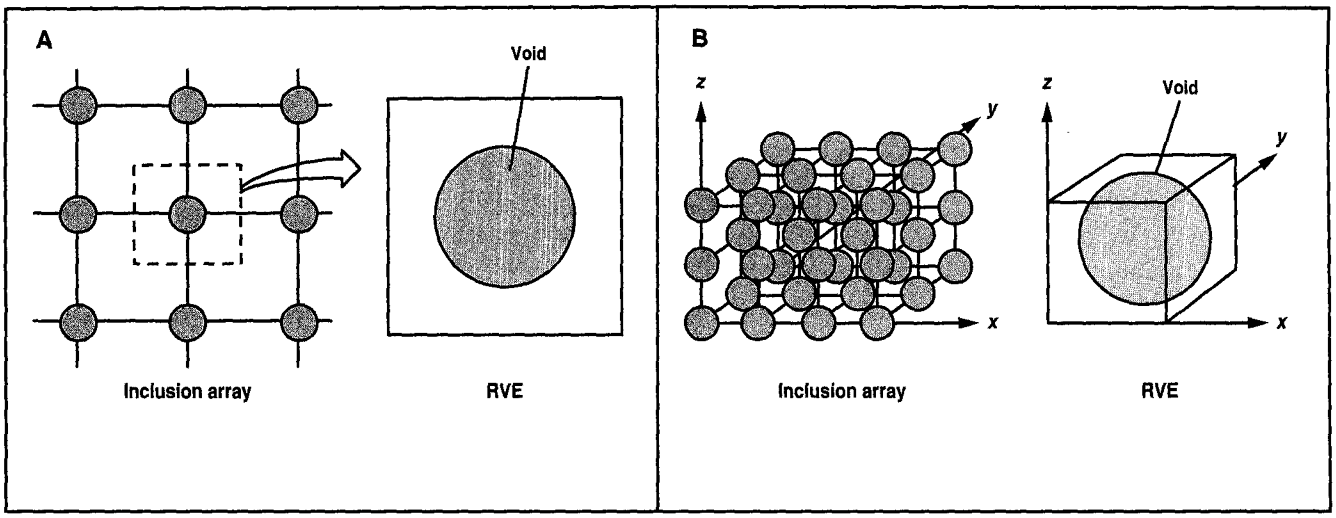

analysis was performed by maintaining constant y-directional displacements of the nodes along the horizontal boundaries AE and BC of the RVE through coupled boundary conditions. The vertical boundaries DE and AB were also constrained to remain straight to guarantee compatibility with the neighboring RVEs after deformation. A uniform stress was applied on the edge AB, and the displacements in the x and y directions, Δx and Δy, were recorded. The effective elastic modulus, E_x, of the porous material can be calculated as follows.

$$E_x = \sigma_x/\varepsilon_x \qquad (3a)$$

with

$$\varepsilon_x = \Delta x/a \qquad (3b)$$

in which a is half the side length of the RVE. Poisson's ratio, ν_{xy}, can be calculated from Eq. 4.

$$\nu_{xy} = -\Delta y/\Delta x \qquad (4)$$

Young's modulus, E_y, was similarly computed by applying a stress σ_y on the edge AE.

To represent shear loading on the RVE, a shear stress, τ_{xy}, was applied on the side AE, as seen in **Fig. 6B.** The side BC was constrained in the x- and y-directions, while the nodes on AE were constrained to have uniform x- and y-directional displacements after deformation. To maintain compatibility with the neighboring RVEs after shear deformation, the edges AB and DE of the RVE should remain straight and parallel. The x- and y-directional displacements of the nodes on side AB were thus constrained to vary linearly from 0 at B to their maximum values of Δx_A and Δy_A at A. The effective in-plane shear modulus of the porous material, G_{xy}, was calculated from the relation

$$G_{xy} = \tau_{xy}/\gamma_{xy} \qquad (5a)$$

where

$$\gamma_{xy} = \Delta x_A/a \qquad (5b)$$

Three-dimensional finite-element analysis

As shown in Fig. 4B, the RVE for a material containing spherical voids is three dimensional (3-D). Solutions for the elastic constants thus require 3-D finite-element analysis. Given the symmetries of geometry, loading, and boundary conditions, only one eighth of the RVE needs to be considered. The RVE was modeled using key points, lines, areas, and volumes *(12)* and discretized using STIF 92 tetrahedral solid elements, as seen in **Fig. 7.** STIF 92 is a ten-noded tetrahedral solid element with three translational degrees of freedom at each node. The mesh generation of the solid can be done automatically in ANSYS *(12)* by specifying either the element size or the number of divisions in each of the line segments of the RVE. In this case, the mesh generation was done by dividing each line segment. Limitations on the memory allocated to the computer system prevented generation of a very fine mesh. Volume fractions of spherical voids ranging from 0.1 through 0.5 (in steps of 0.1) were considered. The corresponding number of elements and nodes generated ranged from 490 to 520 and 1175 to 1225, respectively. The

5. Two-dimensional finite-element discretization of the RVE for cylindrical pores

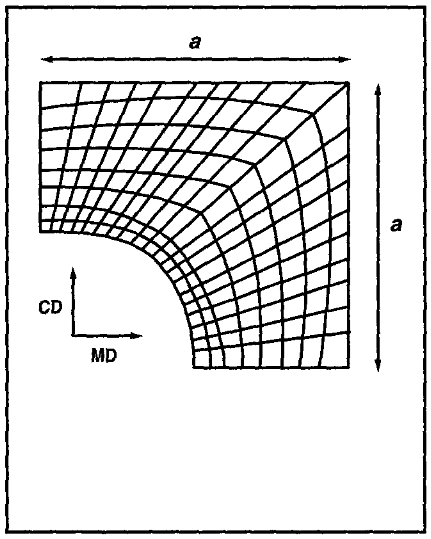

6. Loading and boundary conditions for the RVE for cylindrical pores. **A:** tensile loading, **B:** shear loading.

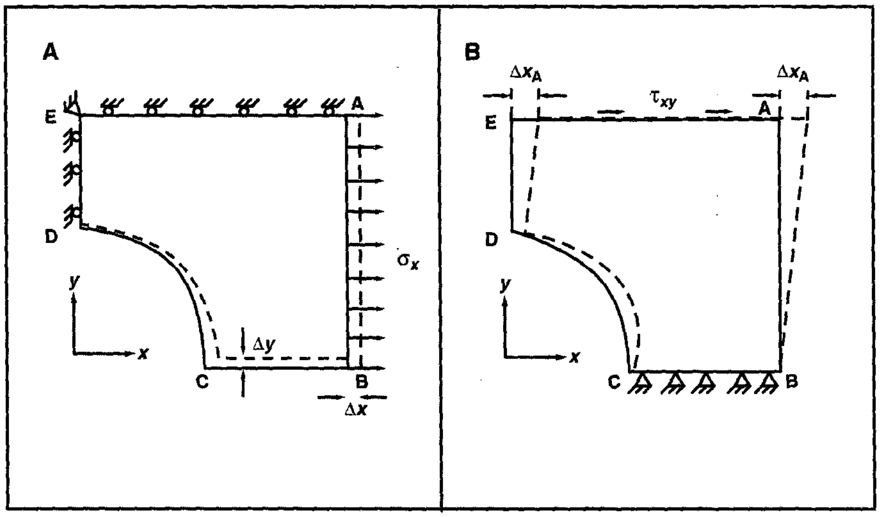

7. Three-dimensional finite-element discretization of the RVE for spherical voids

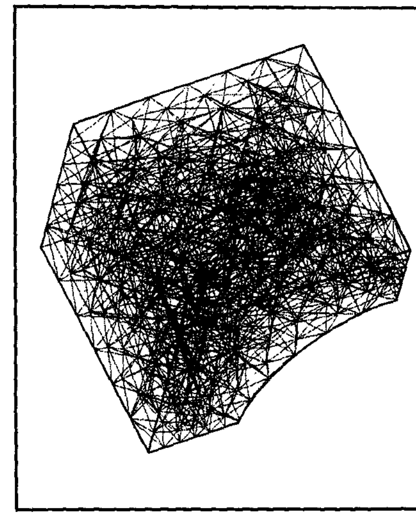

8. Model results (analytical model and finite-element model) showing the effect of void-volume fraction on normalized Young's moduli for a material with cylindrical voids. **A:** modulus in the longitudinal direction, **B:** modulus in the transverse direction.

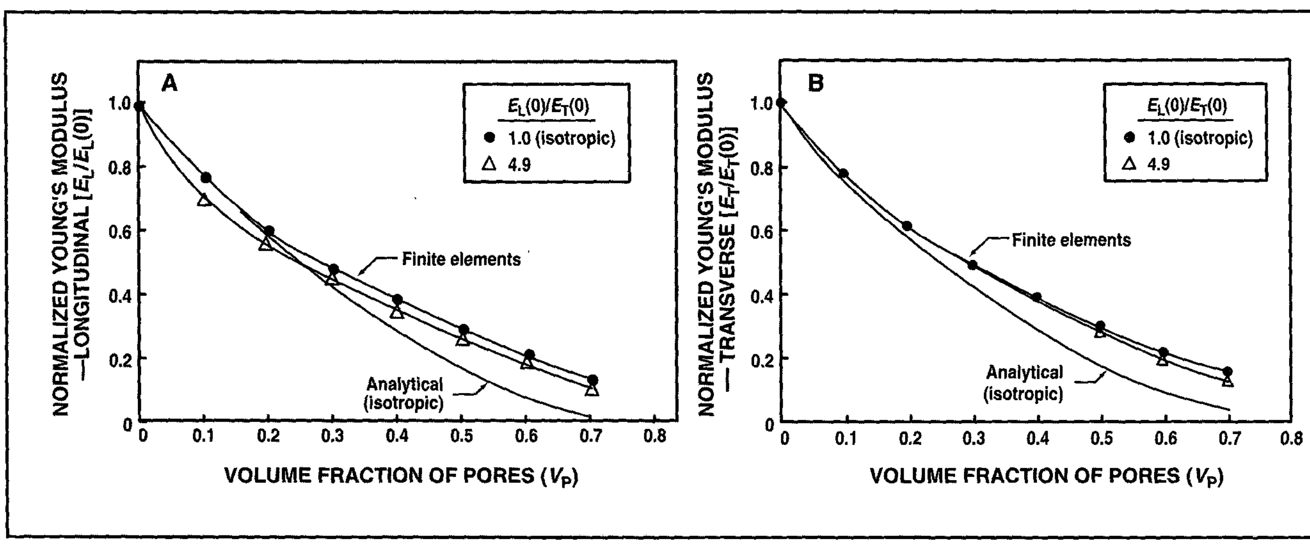

side length of the smallest elements was about $a/8$ for all void-volume fractions, where a is half the RVE side length.

Three-dimensional analysis of orthotropic materials requires all nine orthotropic elastic constants of the matrix (without voids) as input. The in-plane elastic constants for isotropic and orthotropic paper sheets without voids were obtained from the laminate model that was presented in Part 1 *(2)*, although the z-directional properties remain undetermined by the laminate model.

Data on out-of-plane elastic constants of paper are extremely rare, but it should be pointed out that the emphasis of this study is on the in-plane elastic constants, which are not expected to be largely affected by the choice of out-of-plane elastic constants, as long as they are within a reasonable range. Because of the lack of data, the out-of-plane elastic constants of the matrix were selected from the study of Baum *et al. (13)*: E_z = 300 MPa, G_{xz} = 150 MPa, G_{yz} = 200 MPa, ν_{xz} = 0.011, and ν_{yz} = 0.021. These values were assumed to be valid for all of the void-volume fractions and in-plane elastic constants that were considered.

The effective in-plane elastic constants—E_x, E_y, ν_{xy}, and G_{xy}—were calculated by generalization of the procedure outlined for the 2-D finite-element analysis. Details are given in the literature *(14)*. Essentially, compatibility with neighboring RVEs was guaranteed by constraining opposite faces of the RVE to remain planar and parallel after deformation. The moduli and Poisson's ratio were calculated from applied stresses and displacements using Eqs. 3–5.

Results and discussion

Cylindrical pores

The elastic constants calculated for isotropic and orthotropic sheets containing cylindrical pores are plotted vs. pore-volume fraction in **Figs. 8–10.** The results were normalized with the modulus and Poisson's ratio of the material without voids. Comparison of the finite-element predictions for Young's moduli, E_L and E_T in Fig. 8, with those of the analytical model *(8)* (isotropic matrix) reveals that $E_L/E_L(0)$ and $E_T/E_T(0)$—normalized Young's moduli in the longitudinal and transverse directions, respectively—obtained by finite elements are in close agreement with the analytical results at low pore-volume fractions for a material with a modulus ratio, E_L/E_T, close to unity. At higher pore-volume fractions, the analytical results fall below the finite-element results, which may be related to the feature of self-consistent models to underestimate the elastic stiffnesses at large volume fractions *(15)*.

Figure 8 also shows that the anisotropy of the matrix has a small effect on the normalized elastic moduli. The normalized effective moduli slightly decrease with increased anisotropy. The modulus in the longitudinal direction, $E_L/E_L(0)$, decreases somewhat faster with V_P than does the modulus in the transverse direction, $E_T/E_T(0)$, resulting in a slight decrease in the modulus ratio for the porous material, as seen in Fig. 9.

The influence of cylindrical pores on the shear modulus, G_{LT}, is illustrated in Fig. 10A. Again, analytical and finite-element results for an isotropic matrix are in good agreement at low pore-volume fractions, while the finite-element results exceed the analytical prediction at high volume fractions. The normalized shear modulus, $G_{LT}/G_{LT}(0)$, slightly increases with increased anisotropy of the matrix.

9. Effect of void-volume fraction on the anisotropy of paper

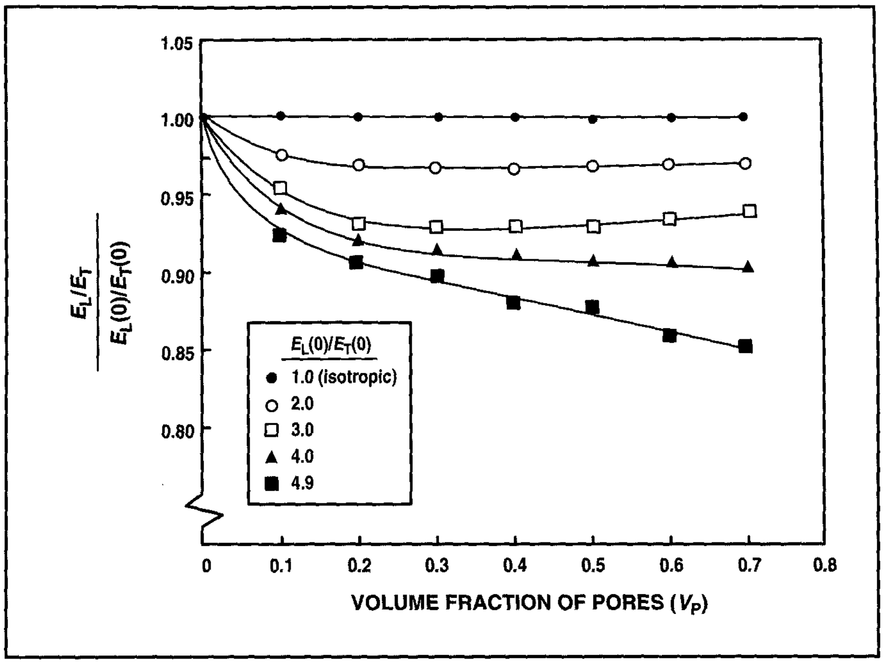

II. Coefficients for polynomial fit of normalized Young's modulus in the longitudinal direction, $E_L/E_L(0)$

$E_L(0)/E_T(0)$	a_1	a_2	a_3
1.0	−2.531	3.375	−2.179
1.5	−2.578	3.533	−2.328
2.0	−2.655	3.736	−2.467
2.5	−2.716	3.895	−2.576
3.0	−2.774	4.057	−2.697
3.5	−2.826	4.190	−2.788
4.0	−2.876	4.319	−2.878
4.5	−2.918	4.408	−2.932
4.9	−3.005	4.715	−3.207

III. Coefficients for polynomial fit of normalized Young's modulus in the transverse direction, $E_T/E_T(0)$

$E_L(0)/E_T(0)$	a_1	a_2	a_3
1.0	−2.531	3.375	−2.179
1.5	−2.405	3.035	−1.962
2.0	−2.318	2.731	−1.702
2.5	−2.347	2.844	−1.806
3.0	−2.346	2.833	−1.793
3.5	−2.382	2.927	−1.861
4.0	−2.406	2.990	−1.902
4.5	−2.473	3.175	−2.035
4.9	−2.521	3.291	−2.109

The finite-element predictions of the normalized Poisson's ratio, $\nu_{LT}/\nu_{LT}(0)$, in Fig. 10B, are relatively independent of the anisotropy·$\nu_{LT}/\nu_{LT}(0)$ predicted by the analytical model agrees with finite-element predictions at low volume fractions, but it increases substantially at larger volume fractions. The discrepancy between analytical and numerical results may possibly be attributed to the regular phase geometry assumed in the finite-element model. The Poisson's ratio for porous materials is very sensitive to the phase geometry *(16)*. As a result, experimental data on Poisson's ratio of porous materials show a large scatter around Poisson's ratio of the matrix *(16)*. Gibson and Ashby *(16)* thus do not recommend correction of Poisson's ratio for the presence of voids, which seems consistent with the results in Fig. 10B.

Spherical voids

Figures 11 and 12 illustrate the effect of spherical voids on the effective engineering constants. The matrix anisotropy does not appre-

10. Model results (analytical model and finite-element model) showing the effect of void-volume fraction on normalized engineering constants for a material with cylindrical voids. **A:** shear modulus, **B:** Poisson's ratio.

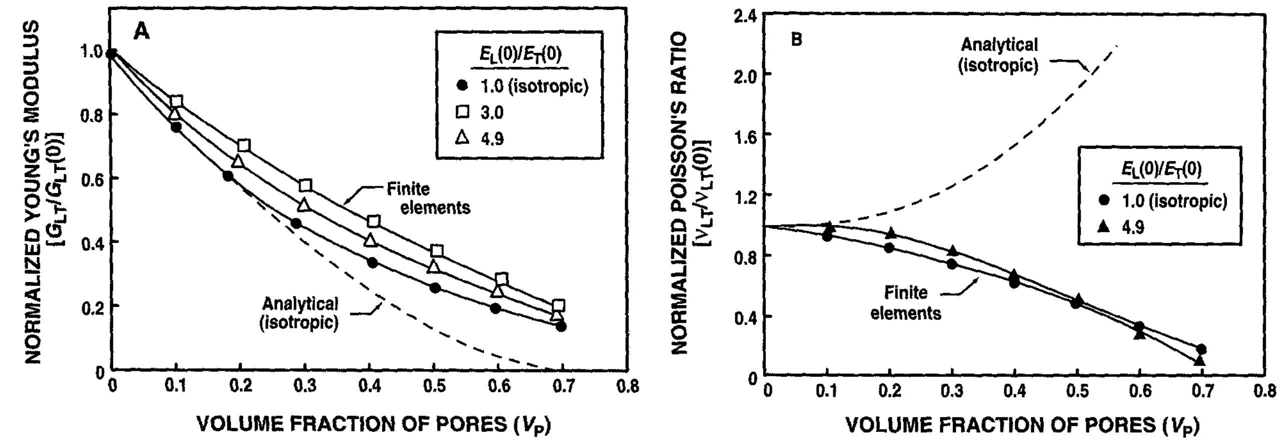

IV. Coefficients for polynomial fit of normalized shear modulus, $G_{LT}/G_{LT}(0)$

$E_L(0)/E_T(0)$	a_1	a_2	a_3
1.0	−2.758	3.675	−2.101
1.5	−2.604	3.297	−1.851
2.0	−2.419	2.848	−1.556
2.5	−2.256	2.458	−1.306
3.0	−2.118	2.112	−1.071
3.5	−1.988	1.758	−0.813
4.0	−1.876	1.475	−0.619
4.5	−1.759	1.186	−0.427
4.9	−1.652	0.953	−0.296

V. Measured Young's moduli for papers produced from bleached chemical pulp (moisture content = 6.3%)*

ρ_S, kg/m^3	E_{MD}, GPa	E_{CD}, GPa	E_{MD}/E_{CD}
783	9.1	5.6	1.6
923	10.7	8.0	1.3
796	11.3	4.0	2.8
940	14.4	5.6	2.6

* Experimental data of Andersson *(19)*

ciably influence the normalized Young's moduli of a material containing spherical voids, as seen in Fig. 11. With increased anisotropy of the matrix, the normalized longitudinal Young's modulus, $E_L/E_L(0)$, decreases, whereas the transverse modulus, $E_T/E_T(0)$, slightly increases. The normalized shear modulus, $G_{LT}/G_{LT}(0)$, and normalized Poisson's ratio, $\nu_{LT}/\nu_{LT}(0)$, increase with increased anisotropy of the matrix, as seen in Fig. 12.

Finite-element calculations of the effective Young's moduli, shear modulus, and Poisson's ratio of an isotropic material with spherical voids are very close to the analytical predictions at low void-volume fractions. At higher volume fractions, the moduli calculated from finite elements exceed the analytical predictions for an isotropic material, while Poisson's ratio calculated by finite elements falls below the analytical results. The elastic constants for an isotropic matrix containing spherical voids calculated by finite elements are generally within Hashin's rigorous bounds *(17)*. Comparison of Figs. 8 and 10 with Figs. 11 and 12 show that the normalized elastic moduli for a material with spherical voids are approximately 10% larger than those of a material with cylindrical voids at a void-volume fraction of 50%.

Hygroexpansion

Finally, the influence of voids on the hygroexpansion coefficients is considered. It can be shown theoretically that voids do not influence the coefficients of hygroexpansion *(18)*. Consequently, there is no need to correct the hygroexpansion coefficients for the presence of voids.

Some useful expressions for cylindrical voids

As discussed earlier, Corte *(5)* considered the pores in a sheet of paper as minute tubes running through the thickness of the material. Hence, the finite-element results for cylindrical pores should be most appropriate for predicting the elastic stiffnesses of paper. To make the finite-element results more accessible, the normalized elastic moduli for a material with cylindrical pores (Figs. 8 and 10) can

11. Model results (analytical model and finite-element model) showing the effect of void-volume fraction on normalized Young's moduli for a material with spherical voids. **A:** modulus in the longitudinal direction, **B:** modulus in the transverse direction.

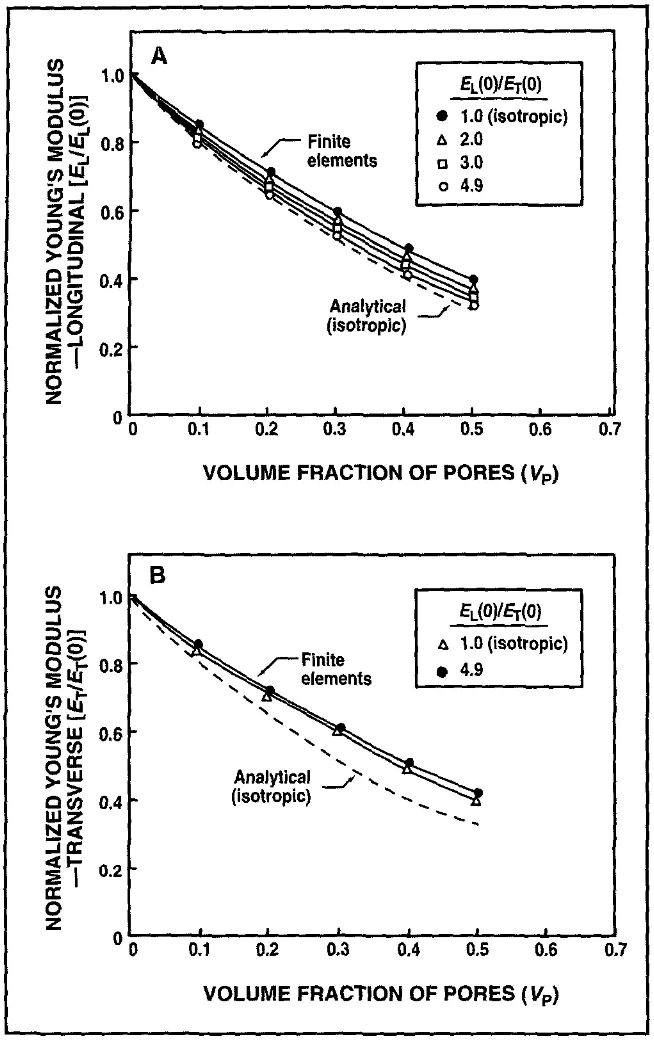

12. Model results (analytical model and finite-element model) showing the effect of void-volume fraction on normalized engineering constants for a material with spherical voids. **A:** shear modulus, **B:** Poisson's ratio.

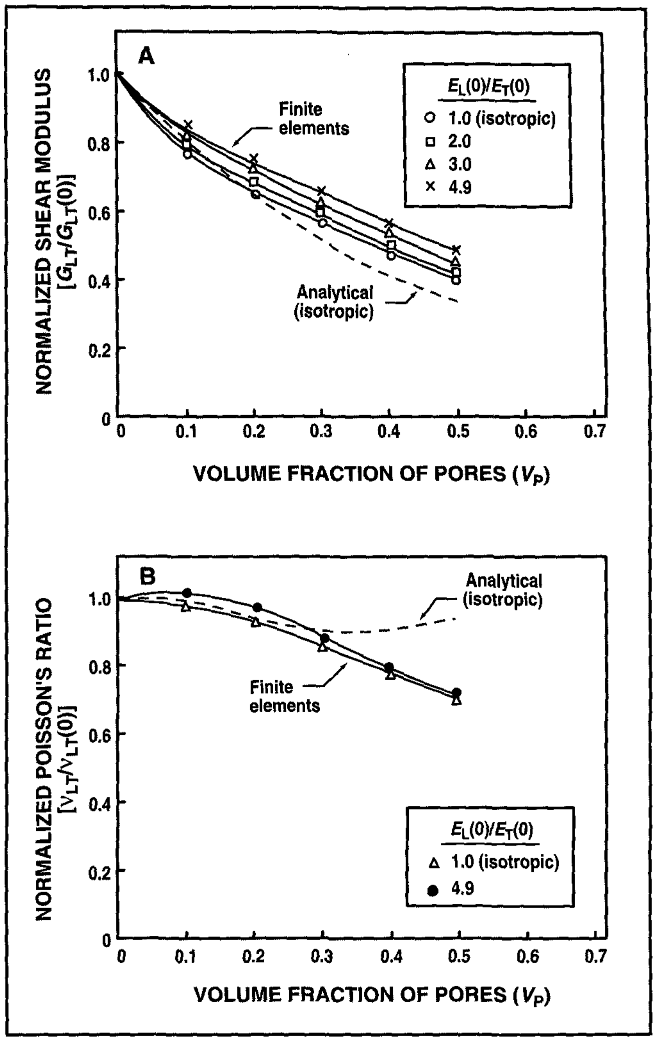

conveniently be represented by the following expression,

$$y = 1 + a_1x + a_2x^2 + a_3x^3 \qquad (6)$$

where $x = V_P$ and $y = E_L/E_L(0)$, $E_T/E_T(0)$, or $G_{LT}/G_{LT}(0)$.

The parameters a_1, a_2, and a_3 were determined by linear regression analysis and are listed in **Tables II–IV**. The correlation coefficients ranged between 0.96 and 1.00, which indicates accurate curve fits.

Correlation with experimental data

Elastic modulus

Consistent experimental data on elastic constants of paper as a function of density are rare. In this section, some available experimental data on elastic moduli of paper sheets are compared with model predictions.

Data on the geometry and distribution of pore sizes in the actual paper sheets considered in the experimental work are not available. According to Corte *(5)*, it is reasonable to expect that the voids may be considered as capillary tubes oriented through the thickness. The pores are thus assumed to be cylindrical, with the axis along the thickness direction. The volume fraction of pores in a paper sheet, V_P, can be calculated from the apparent density, ρ_S, of a paper sheet *(1)*.

$$V_P = 1 - (\rho_S/\rho_C) \qquad (7)$$

where ρ_C is the density of the cell wall [ρ_C = 1500 kg/m^3 *(3)*].

Baum *et al. (13)* studied the dependence of moisture content on the elastic constants of linerboard with a modulus ratio, E_L/E_T, of approximately 2.5 (density range ρ_S = 600–800 kg/m^3). These data are compared with the model results.

13. Calculated and measured *(15)* Young's and shear moduli of linerboard as functions of relative humidity

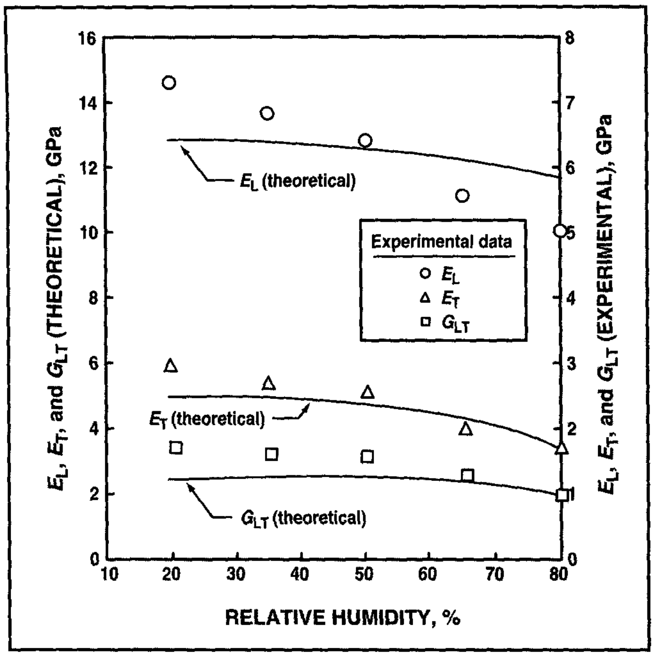

14. Calculated and measured *(15)* Poisson's ratio of linerboard as functions of relative humidity

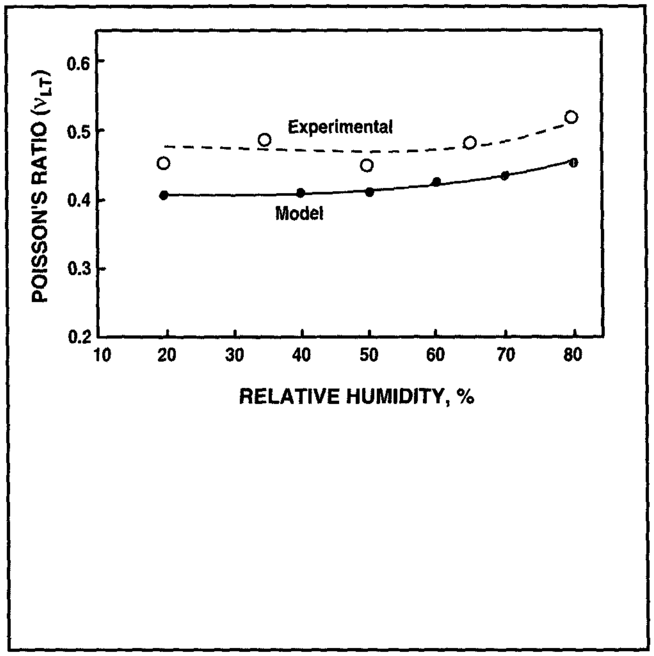

VI. Calculated Young's moduli in the MD and CD for papers produced from bleached chemical pulp (moisture content = 6.3%)

Sheet density (ρ_S), kg/m³	V_P	Baseline $E_L(0)$, GPa	Baseline $E_T(0)$, GPa	$E_L(0)/E_T(0)$	$E_L/E_L(0)$	$E_T/E_T(0)$	E_L, GPa	E_T, GPa
783	0.48	41.0	25.5	1.6	0.301	0.307	12.3	7.83
923	0.39	36.8	28.3	1.3	0.386	0.400	14.2	11.3
796	0.46	56.6	20.2	2.8	0.325	0.340	18.4	6.85
940	0.36	54.6	19.4	2.6	0.400	0.440	21.8	8.54

The elastic constants of void-free paper are first calculated at various moisture contents using the laminate model discussed in Part 1 *(2)*. (See Table II in Part 1.) From the volume fraction of pores calculated from ρ_S using Eq. 7 and linear interpolation of Tables II–IV, the effective elastic constants of papers containing pores were calculated.

Figure 13 shows the effect of relative humidity on the theoretical and experimental elastic constants of linerboard. To simplify comparison, the theoretical and experimental moduli were plotted in different scales (left and right, respectively) that differ by a factor of two (theoretical/experimental). It is found that the moduli obtained from the analytical model exceed the experimental values by a factor of about two. This is a substantial improvement from the results in Part 1 *(2)*, where voids are neglected and the theoretical moduli exceeded the experimental moduli by a factor close to seven. The remaining overprediction of the moduli is most likely due to the assumption of uniform strain in the laminate model, which gives upper-bound estimates of the moduli *(15)*.

The Poisson's ratio (with no correction for voids, as discussed earlier) is close to the experimental values, as seen in **Fig. 14**.

Experimental modulus data for papers made from bleached chemical pulp with a relatively narrow range of sheet densities are presented in **Table V** *(19)*. The baseline Young's moduli in the MD and CD (no voids) were calculated from the laminate model *(2)* by selecting the fibril-orientation parameters so that the modulus ratio, E_L/E_T coincided with the experimental ratio. **Table VI** lists sheet densities, volume fractions of pores, and baseline Young's moduli calculated using the laminate model. The normalized Young's moduli, $E_L/E_L(0)$ and $E_T/E_T(0)$, for the actual pore-volume fractions are obtained from Tables II and III. The calculated effective Young's moduli of the paper sheets are listed in Table VI.

Comparison of the experimental and predicted moduli (Tables V and VI) reveals that the predicted Young's moduli exceed the experimental results. This is again attributed to the assumption of uniform strain in the laminate model, leading to upper-bound values *(15)*.

Hygroexpansion

Hygroexpansion coefficients measured for paper sheets made from chemical pulp *(19)* are listed in **Table VII**. It is apparent that the geometric mean of the coefficients of hygroexpansion, $(\beta_{MD}\beta_{CD})^{1/2}$, is almost independent of apparent density for a given pulp. The experimental data thus support the analytical prediction of invariance of ß with void content.

VII. Measured coefficients of hygroexpansion for papers produced from bleached chemical pulp. (Standard deviations are given within parentheses.)*

Sheet density (ρ_S), *kg/m*^{3}	V_P	E_{MD}/E_{CD}	β_{MD}		β_{CD}		$(\beta_{MD}\beta_{CD})^{1/2}$
780	0.48	1.6	0.17	(0.07)	0.32	(0.11)	0.23
800	0.47	2.8	0.11	(0.09)	0.44	(0.18)	0.22
920	0.39	1.3	0.14	(0.09)	0.22	(0.11)	0.18
940	0.37	2.6	0.11	(0.06)	0.38	(0.16)	0.20

* Experimental data of Andersson *(19)*

Conclusions

Finite-element analysis was used to examine the influence of voids in orthotropic materials. Extensive parametric finite-element analyses were performed to generate elastic stiffnesses of porous materials with cylindrical and spherical voids at various volume fractions and material anisotropies.

The presence of voids results in substantial decreases in the elastic moduli of paper, while the hygroexpansional coefficients are unaffected by voids. The elastic constants normalized with their void-free (matrix) values were found to depend only slightly on the anisotropy of the matrix. The elastic stiffnesses for an isotropic matrix with voids obtained from finite elements were in good agreement with analytical results for an isotropic matrix at low void-volume fractions, but the analytical model underestimates the Young's and shear moduli at high volume fractions.

Based on previous research on the structure of voids, the assumption of cylindrical pores through the thickness of the sheet appears to be most suitable for analyses predicting the elastic constants of paper.

The moduli exceed the experimental values by a factor of about two. The overprediction of the moduli is most likely due to the assumption of uniform strain in the laminate model, which tends to give upper-bound estimates of the moduli. The Poisson's ratio was in closer agreement with experimental values.

Literature cited

1. Bristow, J. A., "The pore structure and the sorption of liquids," in *Paper Structure and Properties* (J. A. Bristow and P. Kolseth, Eds.), Marcel Dekker, New York, 1986, pp. 183–201.
2. Subramanian, L. and Carlsson, L. A., *Tappi J.* 77(11): 209(1994).
3. Salmen, L., Carlsson, L. A., Fellers, C., *et al.*, *Fiber Sci. Technol.* 20: 283(1984).
4. Baum, G. A., "The elastic properties of paper: a review," in *Design Criteria for Paper Performance* (1984 Progress in Paper Physics Seminar Proceedings), STFI, Stockholm, Aug. 1987, pp. 1–27.
5. Corte, H., "Statistical geometry of random fiber network," in *Structure, Solid Mechanics and Engineering Design* (Civil Engineering Conference Proceedings, Part I), Wiley-Interscience, New York, 1969, pp. 341–55.
6. Salmen, L. and Rigdahl, M., *Tappi J.* 68(2): 105(1985).
7. Hashin, Z. and Rosen, W., *J. Appl. Mech.* 31: 223(1964).
8. Christensen, R. M. and Lo, K. H., *J. Mech. Phys. Solids* 27: 315(1979).
9. Adams, D. F. and Doner, D. R., *J. Composite Matl.* 1: 152(1967).
10. Foye, R. L., "An evaluation of various engineering estimates of the transverse properties of unidirectional composites," *Proceedings of 10th National Symposium of the Society for the Advancement of Material and Process Engineering*, SAMPE, Covina, CA, 1966, pp. G31–42.
11. Christman, T., Needleman, A., and Suresh, S., *Acta Metall.* 37: 3029(1989).
12. "ANSYS Engineering Analysis System User's Manual," Vols. 1 and 2, Swanson Analysis Systems Inc., Houston, PA, 1987.
13. Baum, G. A., Brennan, D. C., and Habeger, C. C., *Tappi* 64(8): 97(1981).
14. Subramanian, L., "Analysis of the influence of voids on the hygroelastic properties of paper," M.S. thesis, Dept. of Mechanical Engineering, Florida Atlantic University, Boca Raton, FL, August 1993.
15. McCullough, R. L., "Micro-models for composite materials—Continuous fiber composites," *Delaware Composites Design Encyclopedia*, Vol. 2, Technomic, Lancaster, PA, 1991, pp. 49-92.
16. Gibson, L. J. and Ashby, M. F., *Cellular Solids—Structure and Properties*, Pergamon, New York, 1988.
17. Hashin, Z., *J. Appl. Mech.* 29: 143(1962).
18. Hashin, Z., *J. Appl. Mech.* 46: 543(1979).
19. Andersson, Y., "Micromodel of Paper," Diploma work report, Dept. of Engineering Physics, Chalmers University of Technology, Sweden, 1993.

The authors wish to acknowledge the financial support of the TAPPI Foundation (Pe-96-93). Thanks are also due to Alf de Ruvo of SCA Research, Sweden, for providing additional support. Finally, the authors gratefully acknowledge the Dept. of Ocean Engineering at Florida Atlantic University for the use of their computational facilities.

Received for review Jan. 25, 1994.

Accepted June 22, 1994.

Research for this paper was supported through funding by the TAPPI Foundation. It is the second of many papers resulting from Foundation support that will be published in *Tappi Journal.* For information on the Foundation, call (404) 446-1400, ext. 266 or 211.